Jagiellonian University in Kraków
Faculty of Physics, Astronomy and Applied Computer Science

Anna Miś
Student number: 1127965

Characterization of gamma quanta detector for the SABAT sensor

Master thesis
Field of Study: Advanced Materials and Nanotechnology

Thesis written under the supervision of
dr Michał Silarski
Department of Experimental Particle Physics and Applications

Kraków, 2020

ACKNOWLEDGMENTS

I would like to thank everyone who contributed to this thesis.

First of all, I would like to thank Dr Michał Silarski, for giving me the opportunity to work under his guidance. I am grateful for the inspiration, imparted knowledge and a great understanding. I appreciate his patience in correcting my mistakes during the last three years. Without his inestimable help, finishing this thesis would be completely impossible.

I also thank Dr Szymon Niedźwiecki for his suggestions and help in the laboratory.

I would also like to extend my appreciation to Franciszek Sobczuk for taking measurements together, for valuable comments and IT assistance.

Finally, I wish to thank my Parents primarily for patience throughout these years. Thank for having always believed in me and mobilized me.

Special thanks to Mateusz for forbearance and for always being there for me.

Abstract

The aim of this work was to characterize scintillation detector with LaBr3:Ce:Sr crystal for SABAT project, involving the use of neutrons in the detection of hazardous materials. Such a detector has the best energy resolution among such materials.

The performed research included measuring energy resolution for standard radioactive sources (^{22}Na, ^{137}Cs, ^{133}Ba, ^{60}Co and ^{152}Eu) and for elements activated by fast neutrons (in AmBe source) emitting high energy gamma quanta. The performed measurements concerned such quantities as: energy resolution, time resolution, light attenuation length and light output. The energetic resolution for the Cesium line (662 keV) was about 3%. This is the best result that can be obtained when using a crystal as a scintillation material. Taking into account the results of the energy resolution, its dependence on the energy of gamma quanta was plotted and parameterized. Also plotted how the results depends on the distance between crystal and collimator with source. The study showed that such a detector is linear. The measurements of light attenuation length revealed, that for higher vlotages the charge output of the detector decreases exponentially with decreasing distance of irradiation point to the photocathode.

Contents

1. Introduction

In the 20th century, during the World War II, many new chemical substances serving as warfare were invented. After the war, there were no methods for their effective utilization, so it was decided to get rid of this illict materials by sinking it in the Baltic Sea. Only till 1948 about 25000 tones of arsenal was sunk and nowdays this number is estimated at 62000 tones of dumped munitions [10]. Among them were mustard gas ($C_4H_8Cl_2S$), adamsite ($C_{12}H_9AsClN$), chloroacetophenone (C_8H_7ClO) and hydrogen cyanide (HCN) sometimes called prussic acid.
They are very dangerous and life threating, especially when containers with chemical substances corrode and their contents get into the water. There were a few accidents when it was necessary to evacuate people from the coast of the Baltic Sea. For example in 1955 in Darłówek there was a pollution in which tens of children on the beach were injured [10]. Nowdays, still old munition has been found accidentally. The procedures of neutralizing them include information to the Maritive Office and final recognition by qualifield experts if the object is hazardous or not. The commonly used methods of identification of dangerous substances are based on sonars and magnetometers, they are not effective, costly and often dangerous [10]. For this reason new solutions are needed to identify and locate the hazardous materials on the seabed.
First of all, these methods should be non-destructive and should allow to identify organic substances consisting mainly of carbon, oxygen, hydrogen and nitrogen since most of the hazardous materials are made of these elements. One of the methods which could replace or support the commonly used metods is the neutron activation. There are already several devices that allow for object identification using neutrons. They are based on stoichiometry analysis, because the stoichiometric proportions of these hazardous materials are well known. The neutron flux iradiates on the test substance and interacts with the nuclei of the elements that build the material. The nuclei are excited and while deexcitation to the ground state they emit gamma quanta which can be detected. Precise information about stoichiometry can be obtained from taking into account probabilities of activation of different nuclei with incident neutrons. The measured content of elements is normalized to the number of atoms of one of them, obtaining the characteristic fractions for the substance. Then they can be compared with known compounds and one can determine if the tested substance is dangerous [11].

There are several devices using this method, some on the land the other under water. One of the devices using the described technique is SWAN, the system of detection explosive materials on land. It is the result of the project at the National Centre for Nuclear Research [12]. The device is a mobile, fast neutron activation analyzer. The SWAN's software is optimize for detection of oxygen, carbon and nitrogen [17]. SWAN has spectroscopic gamma detector ($LaBr_3$) integrated with the photomultiplier.The whole is surrounded by tubular anti-Compton detector [17]. In the aquatic environment one finds many difficulties in using neutrons as a probe for noninvasive detection related mainly to strong background radiation from oxygen and hydrogen. There is only one device built and tested underwater: the UNCOSS

(Underwater Coastal Sea Surveyor) sensor. However, it was optimized to detect only explosives [20].

A new device is being developed at the Jagiellonian University in the framework of the SABAT project [2], allowing for quick and noninvasive detection of hazardous materials under water. It assumes the use of guides for neutrons and gamma quanta with variable geometry. They make it possible to choose a neutron beam illuminating part of the examined object without interacting with the surrounding water. They also apply to the registration of some of the emitted gamma quanta that have not been dispersed in water [11]. Schematic of the device is shown in Figure 1.

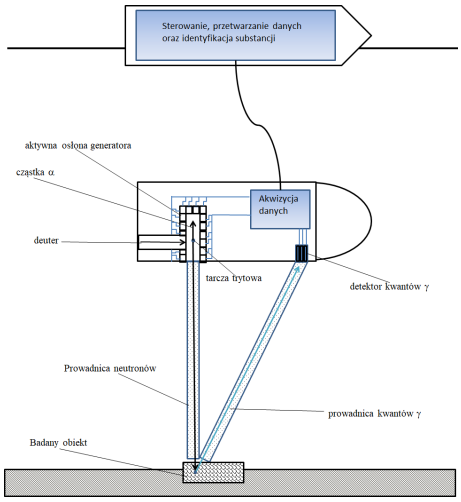

Figure 1: Diagram of the SABAT device [13]

.

1.1 Principles of the SABAT sensor operation

The guides may have the shape of cylinders made of stainless steel, filled with low-pressure air or gas with a low probability of interaction with neutrons. Through collisions of deuterium and tritium in the generator, neutrons and alpha particles are produced. Alpha particles are recorded by a positively sensitive detector installed inside the generator. Neutrons are emitted almost isotropically with a well-defined energy about 14.1 MeV. After leaving the guide, they enter the illuminated object and can be inflexiblely dispersed on the atomic nuclei of the test substance. This amount of energy is sufficient to excite atomic nuclei. During deexcitation they emit gamma quanta with energy specific to this element. Some of the gamma quanta fly towards the detector, inside an analogous guide which, thanks to its specific structure, reduces their absorption and dispersion. Such a detector, for the purpose of reaching particles, should record time, energy and be sensitive to dependent positions. Due to the large neutron fluxes needed for the rapid detection of hazardous substances and the small size of the device, the SABAT project plans to use a scintillation detector to detect the resulting quanta instead of a semiconductor detector [5]. The latter allow to distinguish between lines with very concentrated energies but require continuous cooling and are sensitive to radiation damage caused by neutrons.

Neutrons are neutral subatomic particles that are elements of atomic nucleus. They have no electric charge, so they react almost practically with nuclei. Together with protons they are called nucleons and they account for 99.9 percent of the atom's mass [9].
Neutrons may interact with matter in one of the following reactions:

Elastic scattering
Neutron collides with the nucleus and as a consequence transfer part of its kinetic energy to the atom. Neutron loses more kinetic energy when collides with a light nucleus. This process is crucial in moderation of fast neutrons, e.g. in reactors, and in shielding against neutron radiation [7].

Inelastic scattering
Inelastic scattering is similar to elastic scattering. The difference is when, after the collision, the atomic nucleus has enough energy to go into the excited state. To return to the basic state, the nucleus emitts gamma rays. The entire process takes place according to the reaction [7]:

$$neutron + nucleus \longrightarrow excited\ nucleus \longrightarrow nucleus + neutron + \gamma\ quanta$$

Since the energy states of nuclei are quantized the energies of emitted gamma rays are well defined. Moreover, each isotope has its own, unique set of gamma rays originating from the inelastic scattering of neutrons.

Neutron capture
Low energetic (thermal) neutrons can be absorbed by an atomic nucleus forming a new isotope with increased mass number. For example one can produce ^{60}Co in a thermal neutron capture on the ^{59}Co nucleus. The new isotope is in most of the cases unstable and undergo beta decay followed by emission of gamma rays. Their energies and intensities are again characteristic for each isotope [7].

Charged particle emission
Charged particle emission include two reactions: (n, α) and (n, p). Most of the charged particle emissions (e.g. protons, α particles) occur for fast neutrons, except for two reactions on ^{6}Li and ^{10}B. These reactions are used to convert neutrons to alpha particles or to detect and shield against thermal neutrons [7].

Neutron multiplication reactions
Low energy neutrons can be produced in (n, 2n) and (n, 3n) reactions of fast neutrons on some materials like lead or uranium [7].

Fission
The fission reaction, the basic process, used in nuclear power plants, is a nuclear reaction involving the brake up of a heavy atomic nucleus into two (or more) smaller fragments. These fragments immediately become nuclei of other, lighter elements, e.g. barium and krypton. In addition to fission fragments, neutrons and γ quanta are also emitted. The fission reaction can occur spontaneously or as a result of an interaction with various particles: neutrons, protons, deuterons, α particles, and γ

quanta. Neutrons are most often used because they have no electrical charge, which allows them to easily penetrate the atomic nucleus.
Generally, a heavy nucleus like ^{235}U or ^{239}Pu undergoes fission after absorption of neutron. The nucleus splits into 2 nuclei with emission of 2 – 3 neutrons [7].

2. Gamma radiation detection

2.1 Gamma quanta interraction with matter

Gamma rays are electromagnetic radiation that accompanies some nuclear reactions. It is emitted from the nuclei after their spontaneous decay. Emission of gamma quanta is determined by disparity between final and initial state of the energy levels within the nucleus. Kinetic energy of gamma photon is given by:

$$E = hv = hc/\lambda \tag{1}$$

where: h is Planck's constant, v is frequency of photon, c is the speed of light, λ is the wavelength of radiation.
Depending on the energy, gamma quanta can interact with nucleons, nuclei or electrons in an atom. High energy photons, like gamma quanta, interact with matter by three essential mechanisms: the photoelectric effect, the Compton effect and pair production [5]. Each of them appear in different forms.

Photoelectric effect
In this process gamma quanta interact with an orbital electron bound in an atom. The energy of the gamma quantum is absorbed by the electron that is ejected from its orbit. The resulting vacancy is filled by an external electron. Energy of the electron produced in the photoelectric effect can be expressed as:

$$E_k = hv - E_B \tag{2}$$

where E_B is binding energy of the electron.

Compton effect
Compton scattering is the inelastic scattering of a photon on a loosely bound electron. During the collision photon transfers part of its energy to the electron. The energy of the electron and gamma quanta can be calculated using the conservation of energy and momentum. After Compton scattering, the photon has energy given by the formula:

$$E = hv = \frac{hc}{\lambda} \tag{3}$$

The scattering results in a decrease of momentum of the photon, given by [8]:

$$p_{photon} = \frac{E}{c} = \frac{hf}{c} = \frac{h}{\lambda} \tag{4}$$

It follows that change in photon's momentum must be translated into change in frequency.

Pair production
The pair production is a phenomenon where energy is directly converted to matter [8].
It can be said that pair production is associated with the creation and destruction of matter: annihilation [8]. It consists in the interaction of the particle with the corresponding antiparticle, during which they are converted into photons.

2.2 Gamma radiation detectors

Devices for radiation registration can be divided into two categories, the active and passive detectors. The first of them, immediately send a signal about the passage of the particle, while the second type (passive) uses the fact that the change caused by the passage of the particle can be detected after a while [14].
Passive detectors include dielectric, activation or chemical detectors. Whereas active detectors include: gas detectors (including Geiger-Müller counter, ionization chamber or proportional counter), semiconductor detectors, calorimetric detectors or scintillation counter [14].
The most common detectors are described below.
The Geiger-Müller counter: it usually has the shape of a cylindrical metal tube, inside which, along its symmetry axis, is placed a thin tungsten wire - anode. Along the gas chamber there is a central electrode - cathode. The tube is filled with a suitable gas mixture and is closed in a vacuum vessel. The radiation, e.g. gamma quanta, ionizes the gas in the chamber. The resulting gas ions are accelerated in the electric field and then collide with other atoms, causing further ionization and, as a result, an avalanche discharge. This discharge is manifested by the creation of a voltage pulse, which is directed to the measuring system [15].
The semiconductor detector: A high purity semiconductor crystal (e.g. Ge or Si) reverse polarized by an external voltage. The passage of an ionizing particle induces creation of quasi free electrons and holes which are then drifting in the electric field created due to external voltage and are gathered by electrodes. This results in the appearance of an electrical pulse proportional to the number of charges that have been generated [15]. This kind of detectors provide a very precise determination of the value of the deposited energy, but their timing properties are rather poor due to long charge collection after the particle's interaction.
The scintillation detector: it is based on creation of light, called scintillation, as a consequence of the interaction of an ionizing particle. The advantage of this type of counters is that they register gamma quanta with high efficiency [15]. Due to the fact that the SABAT project will use a scintillation detector, it will be described in detail below.

2.3 Scintillation detector

As already mentioned, this type of counter is based on a scintillation. It is a phenomenon of light formation as a result of the passage of ionizing radiation through some substances. This is due to the absorption of radiation energy and its emission as a result of luminescence.
The scintillation counter consists of a material with scintillation properties combined with a photomultiplier (Figure 2). As a result of the passage of ionizing radiation through the scintillator, its atoms are excited or ionized. Part of the energy is converted into heat, while the remaining part passes from the excited atoms to the crystal's active centers and the emission of photons occurs [16] (detailed description of the scintillation process is given in Chapter 3). The light generated in the scintillator is transformed into an electric signal, which is further processed.

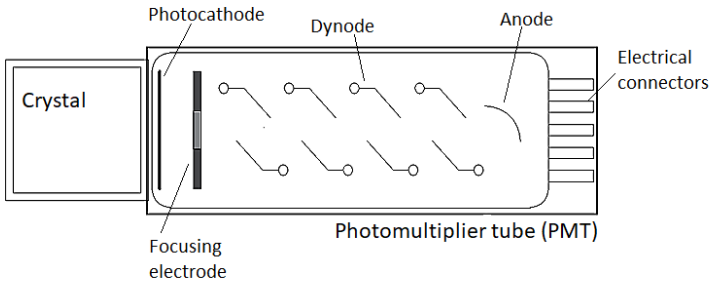

Figure 2: Scintillation detector construction scheme: scintillation material combined with photomultiplier tube which includes an anode, a cathode and a series of dynodes.

Photomultiplier Tube

Photomultiplier tubes are used to convert light into an electrical signal. They consist of a series of dynodes, photocathodes and anodes. As a result of the photon falling on the photocathode, an electron is ejected, which is then accelerated towards a dynode causing a release of additional charges in a multiplication process. Applying several dynodes enhances the number of electrons to a level at which the created electric pulse can be further processed by the Front-End Electronics and Data Aquisition System (DAQ). Photomultiplier gain depends on several factors, such as the number of dynodes, the amount of voltage applied, the type of material from which the dynodes are made and their focusing power.
To ensure that as much as possible of the scintillation light is detected, an optical gel is used to combine the crystal and photomultiplier. In this way, the air gap between them is replaced with a substance with such a refractive index that provides less reflection of the light beam on the border of the two media. Signal from the photomultiplier tube is then amplified by the preamplifier and analyzed, e.g. by a multi-channel analyzer, which allows measurement of the energy spectrum deposited by gamma quanta.

Scintillation is one of the most commonly used methods for detecting ionizing radiation. An ideal scintillation material should meet several criteria, among others should convert the kinetic energy of ionizing into high-performance scintillation light. This conversion should be linear with short decay time. The scintillator should be of good optical quality, appropriate size and transparent for its own emission spectrum, and its index of refraction should be close to the glass refractive index. Unfortunately, no material fulfills all the criteria. The most commonly used scintillation materials are inorganic crystals, organic liquids and plastics. Inorganic scintillators have the best light output and linearity. However, some of them have a slow response time. Organic materials are faster but give less light. The choice of material is often imposed by the type of radiation and application. Inorganic substances are characterized by a high effective atomic number and high density, thus they are a good choice for the detection of gamma radiation.

3. Scintillation process

3.1 Absorption and emission of radiation

Each molecule has a characteristic set of energy levels. As a result of absorption of radiation, the molecule goes into one of the excited states, and then in various ways loses excess energy, which ultimately can lead to electronic transitions, which are accompanied by light emission, called luminescence. It can be concluded that the number of emitted luminescence photons is a good measure of the energy deposited by the absorbed radiation [2]. Absorption and emission processes are schematically represented in Jabłoński diagram in Figure 3. It provides a simplified picture of the relative distribution of the electron energy levels of a molecule and illustrates the intramolecular processes of dissipation of the excitation energy of the molecule following photon absorption and leading to emission, i.e. fluorescence or phosphorescence. The sequence described is as follows: absorption of a photon (A) causes an excitation of a molecule from a singlet ground state (S_0) to one of the singlet excited states (S_1, S_2). The next process is fast internal conversion (IC). This process causes the molecule to move from the excited singlet state S_2 to the excited state S_1. Excited molecule can pass directly from the state S_1 to the ground state S_0 with the simultaneous emission of a photon of energy which is the energy difference between two states. It is a fluorescence process (F). In some situations, it may be a process called intersystem crossing (ISC). This is the transition from the singlet state to the triplet state (T). The return of a molecule from the triplet state to the singlet ground state is called phosphorescence (P). In this process, a emitted photon has smaller energy than the photon emitted in the fluorescence process. Phosphorescence is also a slower process than fluorescence due to the transition between states of different multiplicities, which results in a longer lighting.

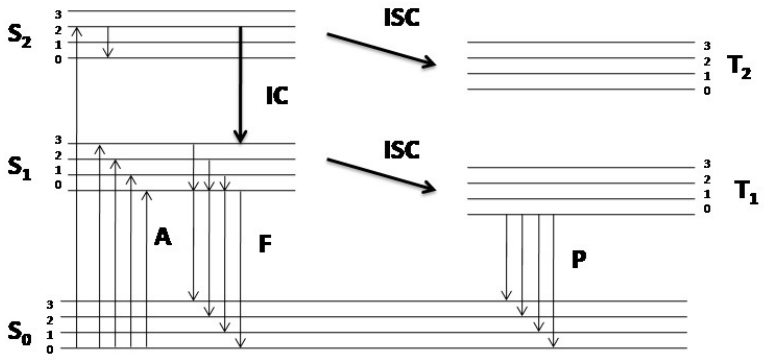

Figure 3: Jabłoński diagram. S_0 means singlet ground state, another singlet states are labeled as S_1 and S_2, while triplet states are marked as T_1 and T_2. Radiant processes are: A- photon absorption, F- fluorescence, P- phosphorescence and non-radiative processes: IC- internal conversion and ISC- intersystem crossing.

There are several processes that can lead to visible light emission. One of them is the process of fluorescence, which is a fast emission of visible radiation from the substance after the excitation. Delayed fluorescence gives the same emission spectrum as fast fluorescence, but again it has a much longer emission time after excitation. Another process called phosphorescence corresponds to the emission of light with a longer wavelength than fluorescence and with a characteristic time that is much slower. To be a good scintillator, the material should transfer as much of the incident radiation energy as possible to accelerate fluorescence while minimizing the overall undesirable phosphorescence and delayed fluorescence.

3.2 Scintillation mechanizm in inorganic crystals

At the atomic level, pure inorganic scintillator crystals exhibit a repetitive crystal lattice. Luminescence is a property of crystal lattice, which determines discrete energy bands available for the electrons. Energy band in an ideal crystal is shown at Figure 4.

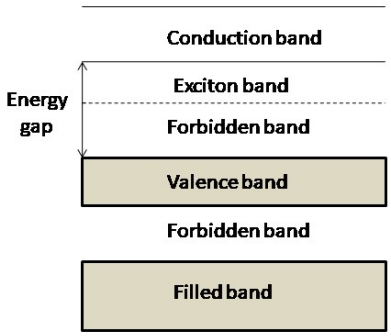

Figure 4: Energy bands in an ideal insulating crystal. From the top: Conduction Band: there are free electrons which tend to move towards neighboring atoms; Forbidden Energy Gap: is between valence band and conduction band, electrons, while going from Valence Bandto the Conduction Band, pass through this and no electron stays there; Conduction Band: band which contains conduction electrons.

Scintillation mechanism in inorganic materials depends on the energy states determined by the crystal lattice of the material. The diagram is presented in Figure 4. The lower band, called valence or primary, means the electrons that are bound at lattice sites, while the conduction band represents those electrons that have sufficient energy to move inside the crystal (being consequently free charge carriers). Levels outside the permitted bands in which the electrons cannot be located are called forbidden bands. During energy absorption, the electron can be transferred from the valence band to the conduction band, leaving a hole in the valence band. In a pure crystal, the process of returning of the electron to the valence band with photon emission is inefficient. Moreover, the gap width determines the energy of the resulting photon that would be too high to appear in the visible range. To increase the likelihood of photon emissions in the visible range small amounts of impurities,

called activators, are added to inorganic crystals. The presence of an admixture in the crystal is benecial because an additional atom can be ionized and provide holes. These impurities cause disturbances in the crystal lattice and, consequently, modification of the crystal's energy band. As a result, they introduce additional energy levels inside the forbidden gap. Thus photon can be emitted in the visible range and serve as the basis for the scintillation process. The charged particle generated in the gamma quantum interaction with the scintillator material is passing through the scintillator and excites electrons from the valence band to the conductivity band and as a consequence a large number of electron-hole pairs are created. The positive hole drifts to the activator and ionizes it because the ionization energy of the activator will be less than the ionization energy of the pure crystal atoms. The electron can move freely in the crystal until it encounters an ionized activator. At this point, the electron can fall into the activator's place, creating a neutral configuration that can have its own set of energy states. If an excited state is created with a permitted transition to the ground state, the transition will occur very quickly and with a high probability of emission of the appropriate photon. For a properly selected activator the transition may be in the visible range.
However, the described phenomenon is not the only one that can occurs in a crystal. Among others, the electron after reaching the pollution site can create a configuration which transition to the ground state is prohibited. An additional energy increase is then required to raise it to a higher state from which a transition to the ground state can proceed. One of the sources of this energy is thermal excitation, and the resulting light is called phosphorescence. The described process can be a source of background or glow in scintillators. As an alternative to the electron and hole migration described above, the pair can move together in a configuration known as the exciton. In this case, the interconnected electron and hole can move freely in the crystal until they encounter an activator atom. At this time, an activator configuration can be created that will cause scintillation when excited.The performance measurement of the scintillation process results from energy calculations. For a wide group of materials an average of about three times the band gap energy is needed to form one electron-hole pair.

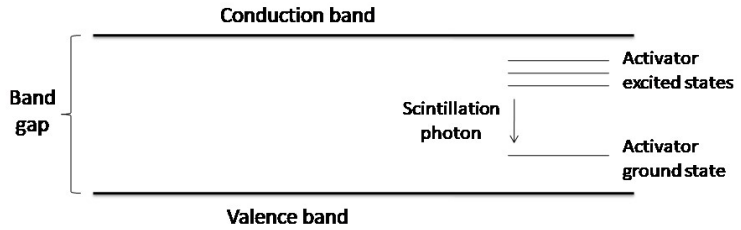

Figure 5: Energy band structure of an activated crystalline scintillator.

3.3 Scintillation materials

3.3.1 Properties of Scintillator Crystals

The choice of a scintillator crystals for a particular application is a compromise between different parameters. The characteristic of the most commonly used scintillation crystals are presented below.

Light yield

The light yield, or light output, is a measure of the amount of light emitted by a crystal per unit of energy [4]. Often light yield is measured as number of emitted photons per deposited energy. In general the more light is emmited by the scintillation material, the better its properties are (e.g. resolution of the measured gamma quanta energy) [4].

Energy resolution

Energy resolution is a parameter that indicates to what extent the detector is able to distinguish photons with similar energies [4]. For a gamma quantum of a given energy it can be defined as the full width at half maximum E_{FWHM} of a peak corresponding to full energy absorption in the detector divided by the energy of the gamma ray which should correspond to the position of the peak E_0, and it can be expressed as:

$$R = \frac{FWHM}{E_0} \cdot 100\% \tag{5}$$

The relationship between the energy resolution and the standard deviation of the measured photopeak is expressed as:

$$E_{FWHM} = 2,35 \cdot \sigma \tag{6}$$

Energy resolution of a scintillator detector is closely connected to the number of photons detected by the photomultiplier [4]. A larger number of photons gives lower relative uncertainty and consequently better energy resolution.

Decay time

The decay time is a parameter determining the time required for scintillation emission to decrease to e-1 of its maximum. The decay time affects the timing properties of the crystal. Shorter decay time decreases the dead time and pileup rate of the detector. It also implies a shorter signal time, so that the time resolution of the detector system is better.

Attenuation coefficient

The attenuation coefficient of a scintillator shows if the crystal is an effective absorber of the gamma photons [4]. Large attenuation coefficient is important for a scintillator material since it determines the efficiency of the gamma rays detection, it depents on the effective atomic number of the material, on its density and on energy of the radiation. Attenuation coefficient is higher when the crystal is of high density and has a high atomic number. The probability that the photon did not

interact travelling a distance x in the crystal is expressed as: [4]:

$$P(x) = e^{-x/\lambda} \tag{7}$$

where λ is the linear attenuation coefficient. Thus, it can be defined as the thickness of the material which attenuates the initial beam of gamma radiation by a factor of e.

Time resolution The time resolution is determined primarily by the characteristics of the charge collection process [1]. The best timing can be achieved with detectors with a fast and constant rise time. Detectors with better timing performance have an equal rise time and produce the highest signal. Slower scintillators can show time resolution values of about 2 ns if pulses of constant amplitude are involved. However, they will have poor timing performance if pulses with a wide amplitude range are processed. Proportional counters have poorer timing resolution because of the variability of the pulse rise time and slower charge collection [1].

Rise time The rise time is time required to change the signal from low to high value [18]. It has been shown that there is a relationship between the Ce concentration in the $LaBr_3$:Ce crystal and rise time [19]. As the doping increases, the rise time decreases.

Others

To choose a scintillation material to appropriate use, there are also other important factors. These include: the refractive index of the crystal, hygroscopic, ruggedness and price [4].

3.3.2 Inorganic Scintillator Crystals

Alkali halide scintillators

The representative of this group is hygroscopic Sodium Iodite doped with Thallium, **NaI:Tl** crystal. It is taken as a typical crystal scintillation material for gamma-ray spectroscopy. The most considerable property of this material is its light yield, about 38 photons/ keV [3]. NaI:Tl, just like other inorganic crystals, shows disproportion of scintillation response with deposited electron energy [1]. The decay time of scintillation pulse is about 230-250 ns [1, 3], which is too long for high counting or fast timing. Energy resolution for ^{137}Cs is about 7,0% [3] and its density amounts to $3{,}7 g/cm^3$ [3].

Other Slow (>200ns) Inorganic Crystals

An example of this group can be non-hygroscopic material Bismuth germanate **BGO** ($Bi_4Ge_3O_{12}$). This is a popular and commercially available crystal with sensible size. It is characterised by high density of about 7,13 g/cm^3 [1, 3] and great effective atomic number (73) because of the bismuth component [4]. These properties results in large probability of the photoelectric absorption of gamma rays. Light yield of this crystal is comparatively low and is approximately 10-20% of NaI:Tl [1]. The decay time of BGO amounts to 300 ns [1, 3], which is slower than previously described crystal. The energy resolution of this material has been measured as about

17% [4].

Unactivated Fast Inorganics with Low Yield

The representative of this group is Barium fluoride $\mathbf{BaF_2}$, which is known as a scintillation material since 1970 [1]. It is a non-hygroscopic crystal which density is 4,9 g/cm^3 [4]. It is a fast scintillator with very short decay time of about 0.6 ns [1]. This advantage makes material attractive for scintillation detectors in which high detection effi

ciency and a fast response are needed [1]. The light output of this scintillator is about 5% of NaI:Tl [5], so its energy resolution is poorer, about 11,4% [5].

Cerium-Activated "Fast" Inorganics

In the 1980s it was discovered that the cerium activator provides great light yield and could be used in new categories of scintillators. The main decay time of the cerium luminescence ranges about 20-80 ns, depending on the type of the doped material. The crystal which belongs to this group is Lutetium Oxyorthosilicate **LSO**. It was first presented as a scintillator in 1991 [1]. This non-hygroscopic material has sapid properties like a light amounting to roughly 75% of NaI:Tl and fast decay time, about 47 ns [1]. The content of Lutetium, which has a high atomic number of 71 is a big advantage in scintillators used for gamma-ray spectroscopy. Unfortunatelly, the isotope ^{176}Lu is radioactive and gives intrinsic background of approximately 300 counts/s [1]. Typical energy resolution is about 10% [1].

In 2001 there was discovered a new scintillator material $\mathbf{LaBr_3{:}Ce}$ that has great properties like excellent energy resolution of about 3% and short decay time of 15 ns [4, 6]. These properties depend on the temperature and Cerrium concentration [6]. Of course, there are drawbacks like lower density (5,1 g/cm^3) and hygroscopic properties because of which crystal is degraded by being exposed to humidity, so it must be sealed.

In later years it was shown that Ca^{2+}, Sr^{2+}, Ba^{2+} dopands were found to affect the scintillation properties of $LaBr_3$:Ce. They improve the energy resolution, light yield and proportionality of the scintillation response. In the literature one can find examples that $\mathbf{LaBr_3{:}Ce{:}Sr}$ has really good energy resolution of 2% at 662keV [6], which makes it the best scintillation material. There could be three different ways to introduce Sr^{2+} into $LaBr_3$Ce: creations of point defects, interstitial cations or Ce^{4+} charge compensation for Sr^{2+} [6]. Due to its superior properties such a material was chosen do build a gamma ray detector for the SABAT project. Its first prototype was built with 2"x2" LaBr3:Ce:Sr crystal connected to a Hamamatsu R7723-100 photomultiplier and will be characterized in the next chapter.

4. Measurements and results

System used in the characterization of the $LaBr_3$:Ce:Sr crystal used as a scintillating material in the SABAT sensor is shown in Figure 6.
As it was mentioned at the end of the previous chapter the crystal was optically connected to the Hamamatsu R7723-100 photomultiplier. An exception was measurement of the light yeld of the crystal when we have used spectroscopic phototube Hamamatsu R6231-100. The photomultiplier was supplied by the CAEN DT5471N power supply. We have used two independent aquisition systems. One of them was CAEN DT5743 digitizer, which allowed for measurement of the full signal waveforms with 250 MS/s sampling rate. The second DAQ system was composed of an Tennelec TC2440 amplifier and Multi-Channel Pulse Amplitue Analyzer TUKAN. The use of positioning system and led collimator allowed for precise formation of gamma quanta beams originating from elemental sources described in the next section.

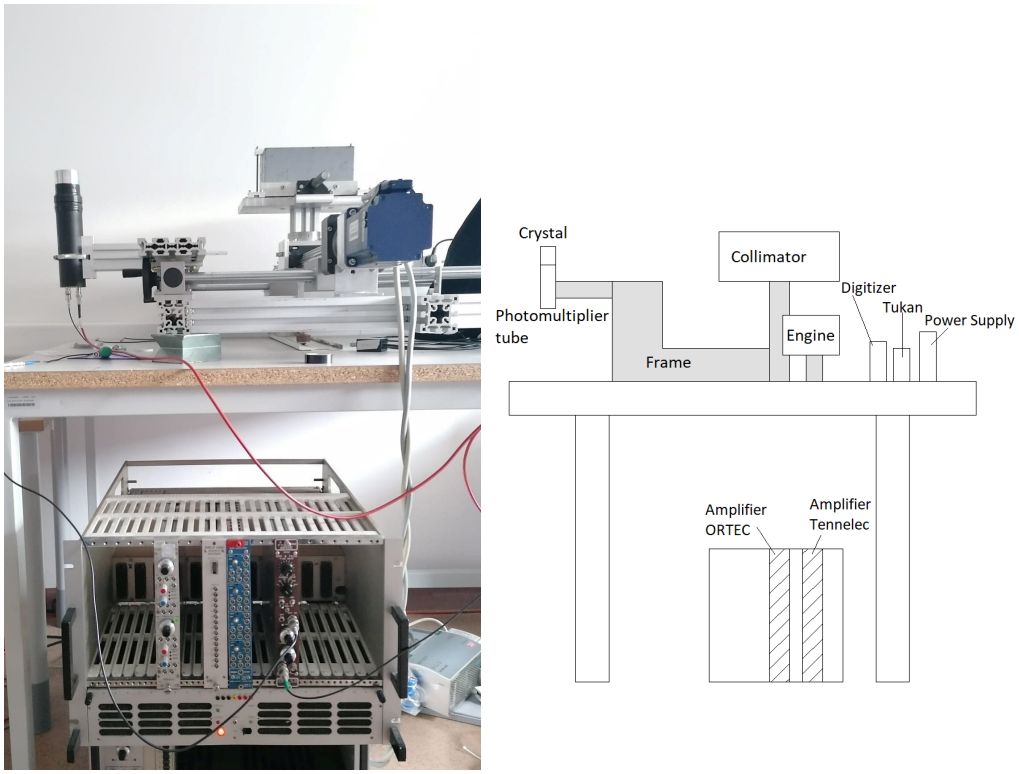

Figure 6: Photography of the experimental setup used in the characterization of the $LaBr_3$:Ce:Sr crystal (left panel) togehter with a schematic representation of the whole system (right panel).

4.1 Radiation sources

In the characterization of the 2"x2" LaBr3:Ce:Sr crystal we have used several sources of gamma rays, both standard calibration sources and isotopes created by activation using neutrons. The standard isotpes used in the measurements were: ^{22}Na, ^{137}Cs, ^{133}Ba, ^{60}Co and ^{152}Eu. Schema of their decay are presented in Figure 7. Deexcitation occurs through the emission of a gamma photon, whose energy is equal to the energy difference between the initial and final nuclear state.
Source ^{137}Cs emits gamma radiation with energy 662 keV. ^{60}Co has two lines and emits photons with energies 1173 keV and 1333 keV. Another source used was ^{22}Na emitting 511 keV and 1274 keV gamma quanta, whereas one of the ^{133}Ba lines has the energy of 356 keV. The last source used was ^{152}Eu, which emits many gamma quanta during decay. The most characteristic are those with energies: 344, 788, 964, 1112 and 1408 keV.

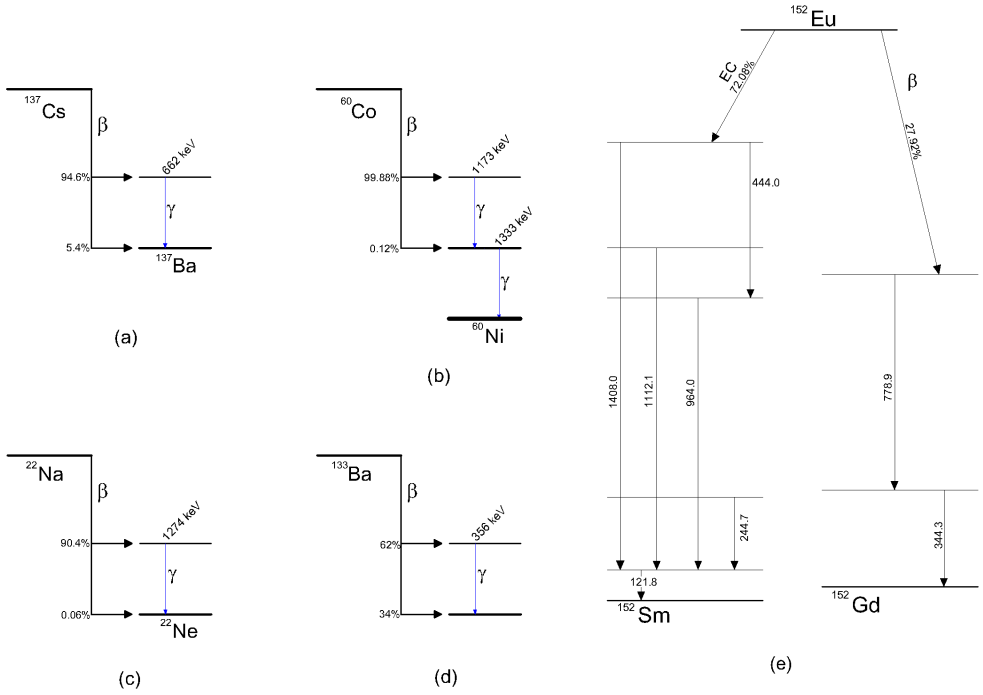

Figure 7: Schemes of radioactive isotope decays used in the study: a) Cesium (^{137}Cs), b) Cobalt (^{60}Co), c) Sodium (^{22}Na), d) Barium (^{133}Ba) and e) Europium (^{152}Eu).

.

An AmBe neutron source was used for research with high-energy gamma quanta. It provides neutrons which are produced after the reaction of Beryllium with an alpha particle originating from the ^{241}Am isotope. The activity of the source was 12,95 GBq and the efficiency of neutron emission amounted to $7{,}7 \cdot 10^5$n/s. The source was placed in a paraffin shield, which at the same time was a source of higher energetic gamma rays, mainly from the neutron capture on hydrogen (E_{gamma} = 2.2. MeV).

4.2 Energy resolution

The scintillation crystal was connected to the photomultiplier. After assembling the apparatus, the appropriate voltage for the photomultiplier tube was applied. The measurement was carried out sequentially with various radioactive sources (described in 4.1).

To determine the energetic resolving power of the detector, we have gathered spectra of the energy depositions for each source described before. We were focused on the full energy absorption peak for all the emitted gamma lines. A fit of the Gaussian function allowed to determine the position of these peaks and their FWHM values. A multi-channel analyzer Tukan was used to collect the data. It is a computer controlled device designed for qualitative and quantitative measurements of the ionizing radiation spectrum from various types of detectors.

To determine the energy resolution for high-energy gamma quanta, a neutron source was used. Peak was observed at 2,2 MeV (Hydrogen). To achieve the lowest background, and consequently also a more accurate measurement, various detector locations were tried: directly on paraffin, on a closed cover and on the ground (Figure 8).

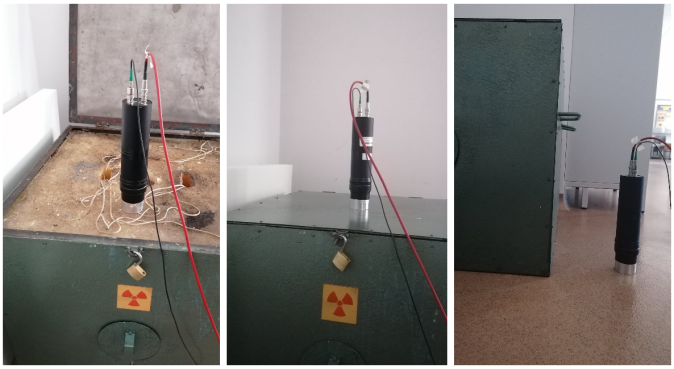

Figure 8: Measurements to check the energy resolution of the SABAT detector at the hydrogen line. Three measurements were done to minimize the influence of the background.

The best result were obtained with the closed lid of the neutron source. Therefore, results of this measurement were taken into account in further considerations.

Since all the measurements were done at the same photomultiplier voltage the central values of the photoelectric peak were used to calibrate the Multi-Channel Analyzer TUKAN and obtain the relation between a channel number and measured energy. This dependence is shown in Fig. 9. As one can see this dependence turns to be linear in the energy range up to 1500 keV.

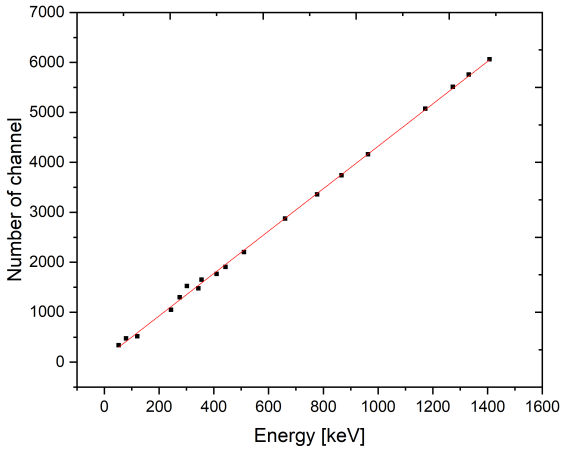

Figure 9: Linear dependence of the channel number on energy.

Perfoming linear regression it tuned out that one can parametrize this dependence with a function given by the formula: $y = a + b \cdot x$
where: a = -17,5 $\pm$ 5,8 and b = 0,2353 $\pm$ 0,0018

This calibration function was applied to all the measured energy spectra for which we have again fitted the full absorption peaks with the Gauss function. This allowed to determine their full width at half maximum (FWHM), and then energy resolution as a function of the gamma quantum energy.

Below are examples of energy distributions measured for the ^{22}Na and ^{137}Cs isotopes.

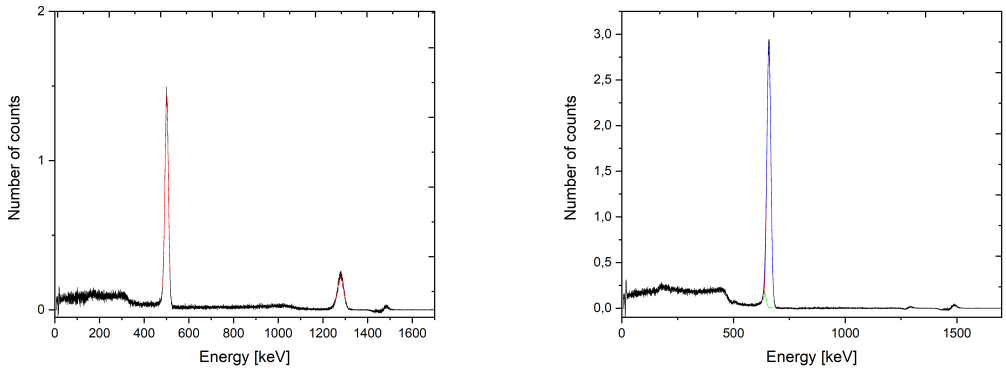

Figure 10: Energy spectra of gamma quanta emitted by Sodium and Cesium sources recorded with a $LaBr_3$:Ce:Sr scintillation detector.

Table 1: Results of the energy measurements for the $LaBr_3$:Ce:Sr scintillation detector for elemental sources.

Element	Energy of γ quanta [keV]	FWHM	R
^{22}Na	511	17,72 ± 0,20	0,03468 ± 0,00039
^{22}Na	1274	29,59 ± 0,83	0,02323 ± 0,00065
^{60}Co	1173	28,69 ± 1,57	0,0245 ± 0,0013
^{60}Co	1333	32,783 ± 3,052	0,0246 ± 0,0023
^{137}Cs	662	20,47 ± 0,31	0,03097 ± 0,00047
^{133}Ba	53	6,153 ± 0,052	0,11609 ± 0,00098
^{133}Ba	80	8,35 ± 0,12	0,1044 ± 0,0016
^{133}Ba	276	12,75 ± 0,13	0,04619 ± 0,00049
^{133}Ba	302	13,89 ± 0,27	0,04599 ± 0,00088
^{133}Ba	356	14,74 ± 0,15	0,04140 ± 0,00042
^{152}Eu	121	7,473 ± 0,085	0,06176 ± 0,00071
^{152}Eu	244	11,13 ± 0,23	0,04561 ± 0,00093
^{152}Eu	344	13,43 ± 0,11	0,03904 ± 0,00031
^{152}Eu	411	14,51 ± 0,58	0,0353 ± 0,0014
^{152}Eu	443	14,77 ± 0,80	0,0334 ± 0,0018
^{152}Eu	778	21,09 ± 0,67	0,02710 ± 0,00086
^{152}Eu	867	19,19 ± 1,99	0,0221 ± 0,0023
^{152}Eu	964	23,68 ± 0,51	0,02456 ± 0,00053

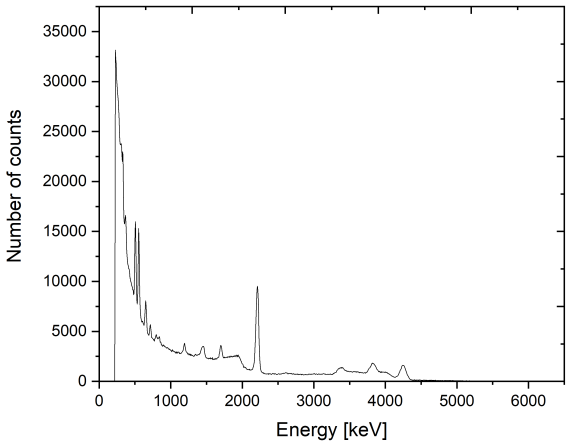

Figure 11: Energy spectra of gamma quanta emitted by neutron source recorded with a $LaBr_3$:Ce:Sr scintillation detector.

Table 2: Results of the energy measurements for the $LaBr_3$:Ce:Sr scintillation detector for the Hydrogen line.

Element	Energy of γ quanta [MeV]	FWHM	R
^{1}H	2,2	42,63 ± 1,53	0,0193 ± 0,0007

Summary of all the results obtained for gamma quanta lines up to about 1400 keV is presented in Table 1 and Table 2. In Figure 12 one can see the energy dependence of the resolution only for elemental sources (left panel) and with the measurement of the Hydrogen line (right panel).

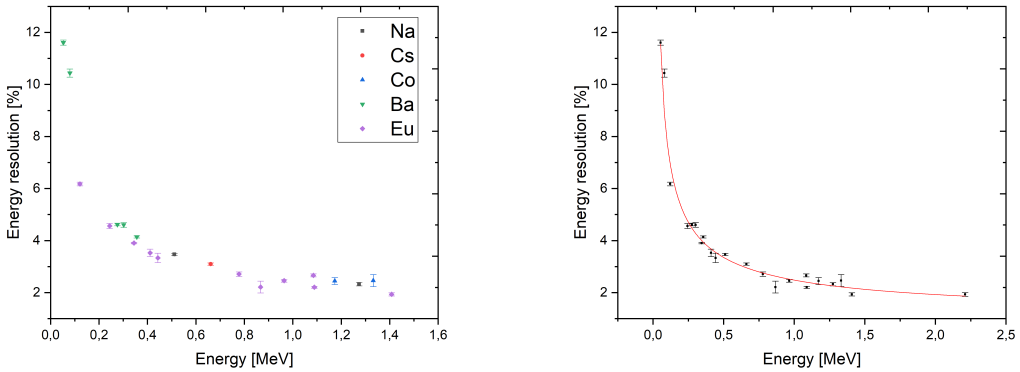

Figure 12: The dependence of energy resolution on gamma quanta energy for standard radioactive sources (left) and with the result for activated Hydrogen (right). The red curve represent a fit to the data using the following function: $y = \frac{\sqrt{a+bE+cE^2}}{E}$.

The whole dataset was fitted with a standard function describing the resolution dependence on energy of the following form (see the right panel of Figure 12):

$$y = \frac{\sqrt{a + bE + cE^2}}{E} \tag{8}$$

where E denotes the gamma-quantum energy in MeV, a = 0,121 ± 0,041 [MeV^2], b = 4,72 ± 0,47 [MeV], c = 1,32 ± 0,68.

As one can see, the parametrization describes quite well the experimntal data and the energy resolution goes down to about 2% for high energy gamma quanta.

4.3 Linearity of the detector response

The linearity of the detector was already partially demonstrated in the previous section where a linear dependence of the TUKAN analyzer and the full absorption peaks was found up to 1400 keV. In this section results of the linearity checks performed also for higher energies and two different voltages are presented. For this purpose, an analysis of the relationship between the literature value of the gamma quanta energy and the experimental value estimated from the photopic centroid was performed. Measurements were for two voltages of the analyzer channel number: 1450V (for ^{22}Na, ^{137}Cs, ^{60}Co and neutron source) and 1550V (for ^{22}Na, ^{137}Cs, ^{133}Ba, ^{60}Co and ^{152}Eu). In both cases, the aforementioned relationship turned out to be linear (Fig.13). A linear function was fitted to both plots. Linear regression confirms that the response of the SABAT scintillating detector is linear.

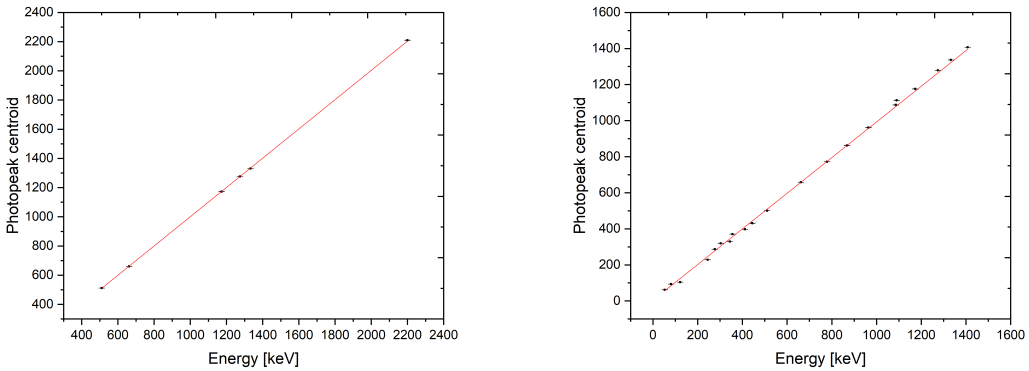

Figure 13: The dependence of the photopeak centroid on the nominal energy of the measured gamma lines for high voltage equal to 1450 V (left panel) and 1550 V (right pannel). The results of the y = a + bx function fits are also given. The estimated parameters amount to a = -2.11 ± 2.1 and b = 0,989 ± 0,016 (left panel) and a = -4,12 ± 4,32 and b = 0,989 ± 0,016 (right panel).

4.4 Energy resolution dependence of the radiation interaction rate

Deterioration of the energy resolution with increasing radiation rate was checked by measurement with strong ^{137}Cs source placed in the lead collimator. The detector load was changed by moving the source towards the detector. The detector was positioned horizontally, so that the crystal and the collimator are parallel to each other (Figure 14).

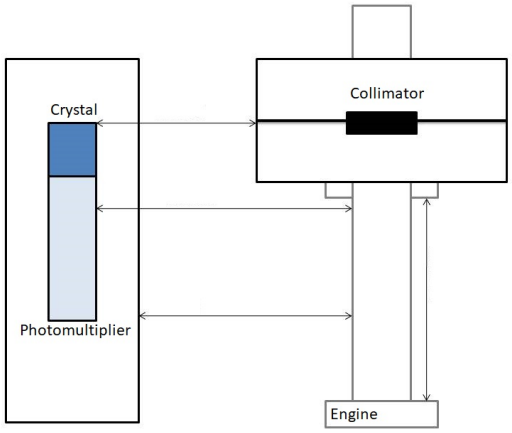

Figure 14: Scheme of the system for measuring dependence of the energy resolution on the detector load.

All measurements were taken with the source into collimator in addition to the last two (0mm, 235mm). Energy resolution value (in %) was determined using the TUKAN Multi-Channel Analyzer. Then, the obtained results were analyzed in the OriginPro and the dependence of the number of counts on energy was plotted for different crystal-collimator distances. The sum of two Gauss function was fitted to the determined photopeaks at each distance (see Figure 15).

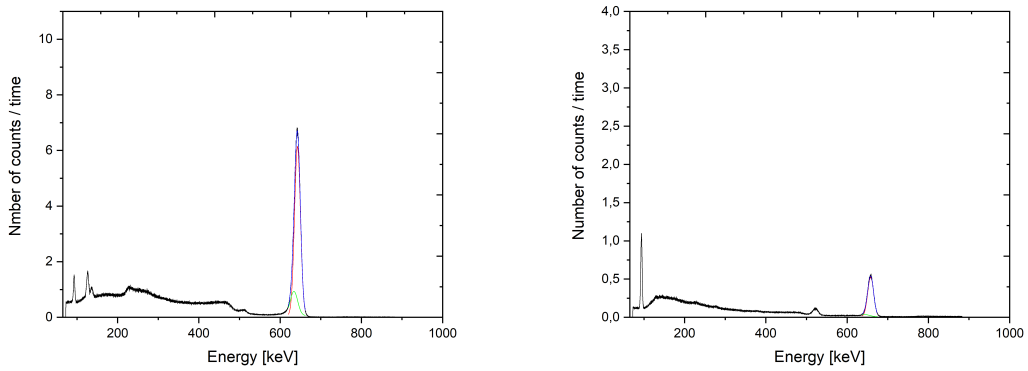

Figure 15: Energy deposition spectra of the ^{137}Cs source measured at a distance of 235 mm (left panel) and 475 mm (right panel). In borth cases the distributions were normalized to the total time of measurement.

Then, on the basis of the obtained graphs, the values of the energy resolution were calculated and the results for different distances were compared in Table 3.

Table 3: The dependence of the energy resolution on the distance between the source (Cs) and the $LaBr_3$:Ce:Sr crystal.

Distance [mm]	Energy resolution [%]
235	2,58 ± 0,15
345	2,59 ± 0,41
355	2,57 ± 0,22
375	2,59 ± 0,14
395	2,50 ± 0,55
415	2,59 ± 0,30
445	2,56 ± 0,04
475	2,61 ± 0,27

The dependence of the energy resolution on distance between crystal and collimator was plotted and linear regression was performed. As one can see in Figure 16 there are no significant differences observed for the measured data.

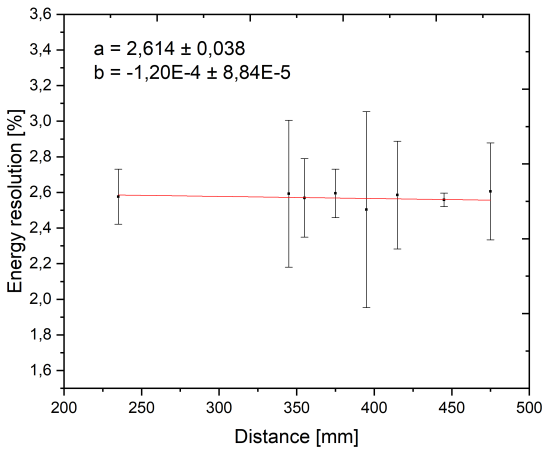

Figure 16: The dependence of the energy resolution on distance between crystal and collimator with linear regression.

4.5 An attempt to measure the crystal light attenuation length

The detector was rotated horizontally. The the 2 mm slit of the collimator was positioned so that the beam irradiated the edge of the crystal (position named as 0 mm). For each measurement the collimator (and in consequence the beam) was moved 5 mm towards the photomultiplier. The crystal length is 55 mm, therefore 12 measurements. These studies were done using the CAEN DT5743 digitizer as the data acquisition system. For each position we have gathered 100000 events consisting of complete waveforms of signals. These waveforms were integrated so that the charge of each registered signal was calculated. As a radiation source a ^{22}Na isotope was used since it provides two gamma quanta lines for which one can study the light attenuation.

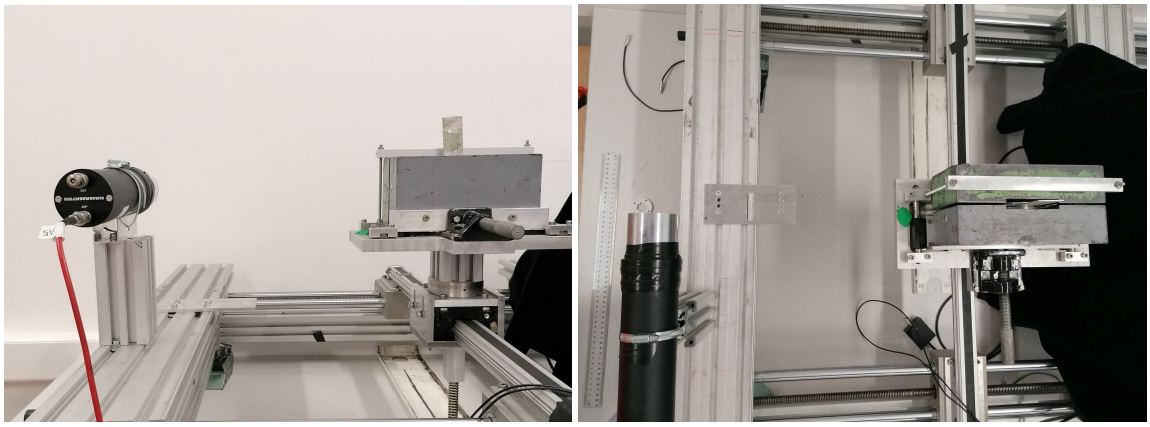

Figure 17: Detection system used to measure the crystal length attenuation.

The calculated charges, histograms of measurements in the OriginPro program were drawn (example in Figure 18). The mean charge corresponding to the two ^{22}Na lines was estimated by fitting the Gauss function.

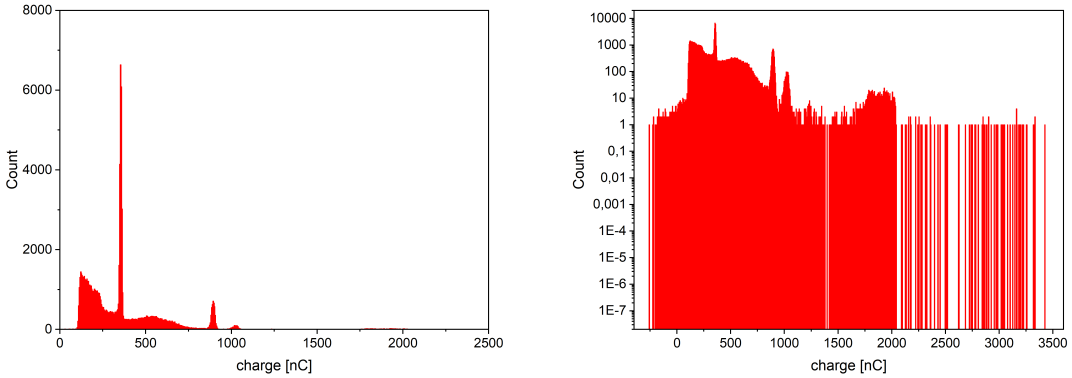

Figure 18: Histograms of the charge collected by irradiating the scintillator at a position of 10 mm from the edge of the crystal showed in the linear and logarithmic scale. The Two peaks of full absorption of the ^{22}Na source is clearly seen. The third maximum originates from the internal radiation of the crystal.

The mean charge of the gamma quanttum photopeak depends on the number of photons reaching the photocathode of the PMT which, in turn, depends on the attenuation length of the scintillator. Thus, change in the registered mean charge should reveal the light attenuation properties of the scintillator. The measured photopeak mean charge in a function of the position of the irradiation is shown for the two studied gamma lines in Figure 19.

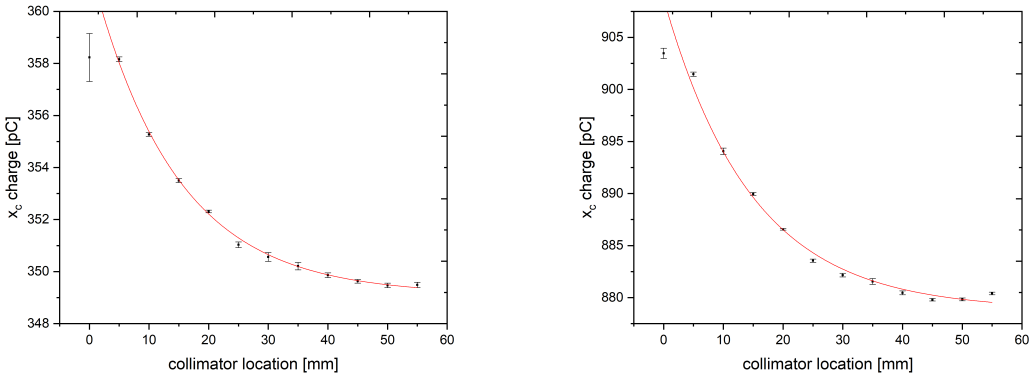

Figure 19: The mean charge of the full absorption peak as a function of the point of irradiation for the gamma quanta with energy of 511 keV (left panel) and 1274 keV (right panel). The red curves represent exponential fit of the form $y = y_0 + A \cdot \exp(-x/R_0)$, with $R_0 = 14$ [mm].

By analyzing the obtained graphs (Figure 19), it can be seen that the charge decreases exponentially as the beam moves deeper into the crystal. This means that the closer the photomultiplier beam hits, the less charge is registered. This may happen if for irradiation position closer to the PMT its gain drops rapidly. To check if this is the reason of observed effect we have done three test measurements at lower high voltage of the photomultiplier.

Control measurements were carried out for the voltages: 1500, 1400 and 1300V at four positions of the collimator. The results are presented below.

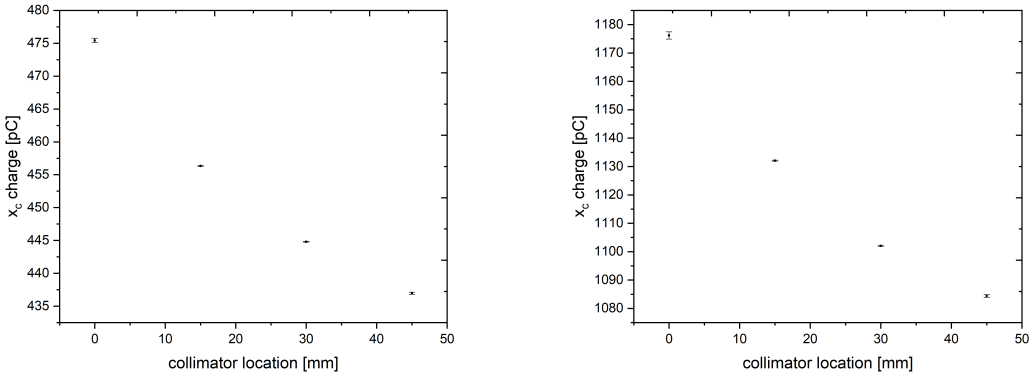

Figure 20: The mean charge of the full absorption peak as a function of the point of irradiation for the gamma quanta with energy of 511 keV (left panel) and 1274 keV (right panel) measured at the PMT high voltage equal to 1500 V.

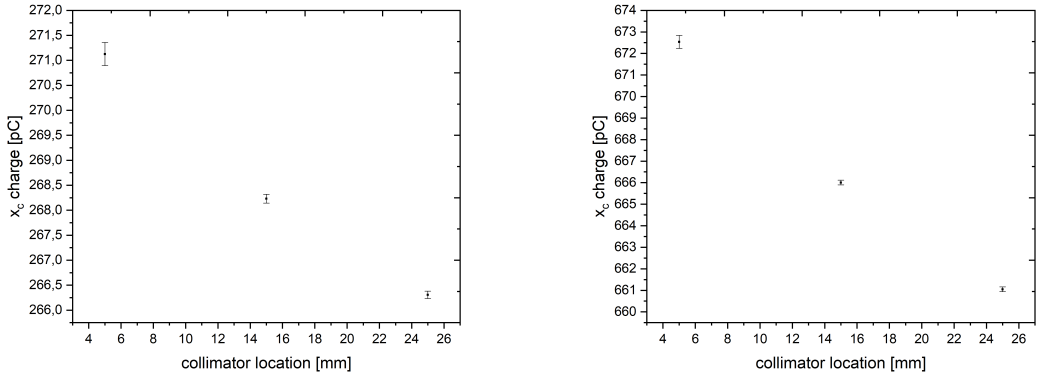

Figure 21: The mean charge of the full absorption peak as a function of the point of irradiation for the gamma quanta with energy of 511 keV (left panel) and 1274 keV (right panel) measured at the PMT high voltage equal to 1400 V.

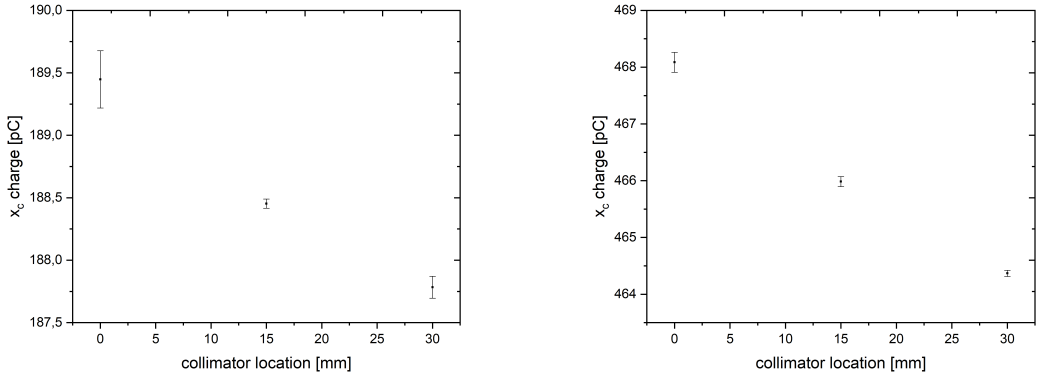

Figure 22: The mean charge of the full absorption peak as a function of the point of irradiation for the gamma quanta with energy of 511 keV (left panel) and 1274 keV (right panel) measured at the PMT high voltage equal to 1300 V.

As can be seen in the above graphs, regardless of the applied voltage, the charge values decrease as the collimator moves (the beam closer to the photomultiplier).

In order to compare the obtained values, they were all placed on one graph. The result is presented in Figure 23. As one can see the exponential dependence of the mean charge of the photopeak on the collimator position gets weaker while lowering the high voltage of the PMT but the real reason of this observation remains unclear. These results suggest that at the PMT voltages grater than 1300 V to obtain the best performance the detected radiation should hit the front surface of the crystal distant from the fotocathode.

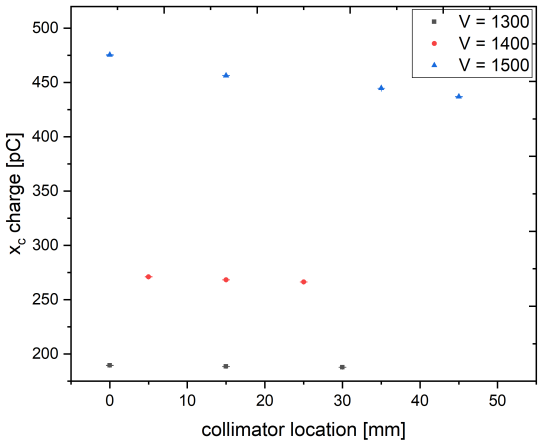

Figure 23: Comparison between the mean charge of the full absorption peak as a function of the point of irradiation for the gamma quanta with energy of 511 keV measured at the three PMT high voltage values.

4.6 Time resolution

The detector was rotated vertically. A second detector was placed horizontally on the other side of the collimator (Figure 24). The measurement was done again using the ^{22}Na source since it provides correlated gamma quanta from positron annihilation. Signals from the SABAT detector were measured in coincidence with the reference detector again using the CAEN digitizer. Measurements were done for several values of the PMT high voltage from 1100 V to 1700 V with step of 100 V.

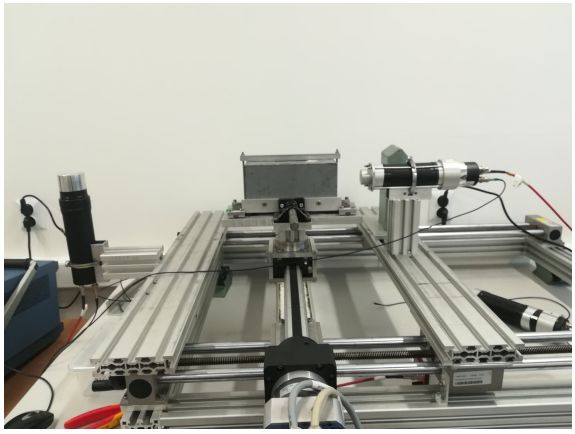

Figure 24: Photograph of the system used to measure the time resolution of the SABAT detector, from left: detector $LaBr_3 : Ce : Sr$, collimator with engine and reference detector.

The arrival time of the reference signal t_{ref} and the arrival time of the SABAT signal t_S was based on the registered waveforms. The time delay Δt between the two signals:

$$\Delta t = t_S - t_{ref} \tag{9}$$

As in other cases the Gauss function:

$$n_T = c \cdot exp[\frac{1}{2}(\frac{\Delta t - t_0}{\sigma_T})^2] \tag{10}$$

is fitted to the histogram of Δt values.
Finally the FWHM of the Δt distribution is calculated using the formula:

$$FWHM_T = 2\sqrt{2ln2} \cdot \sigma_T \tag{11}$$

As expected the obtained time resolution is a descending function of the PMT high voltage as presented in Figure 25.

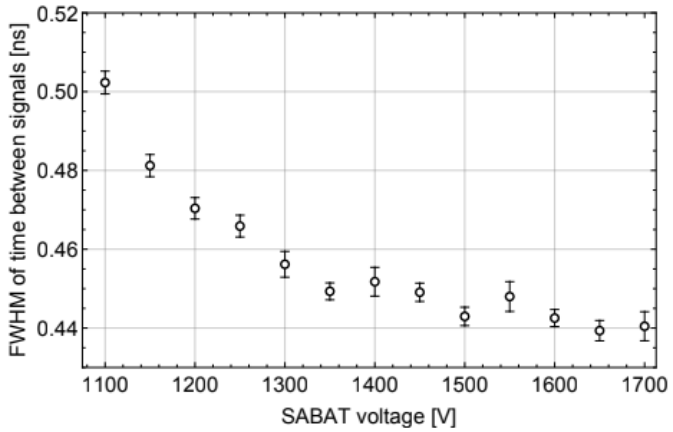

Figure 25: The dependence of the time resolution on the voltage set on the SABAT detector.

4.7 Light output measurement

The crystal was disconnected from the photomultiplier tube. Then, the surface of the photomultiplier was completely darkened so that no light could reach the photocathode. The voltage was applied to the photomultiplier tube and the measurement was made using Tellnec aplifier and TUKAN Multi-Channel Analyzer. This allowed for the registration of a single photoelectron.
After the measurement was completed, the crystal was recombined with the photomultiplier tube by means of an optical gel, and the measurement was performed with a Cesium source. Tukan was also used to record the signal.

Two measurements were taken: first one for the amplifier shaping time equal to 0,25 μs and second one with 0,375 μs. In both cases we have performed the single photoelectron and the ^{137}Cs spectrum measurement. Results of these two measurements are presented in Figure 26.

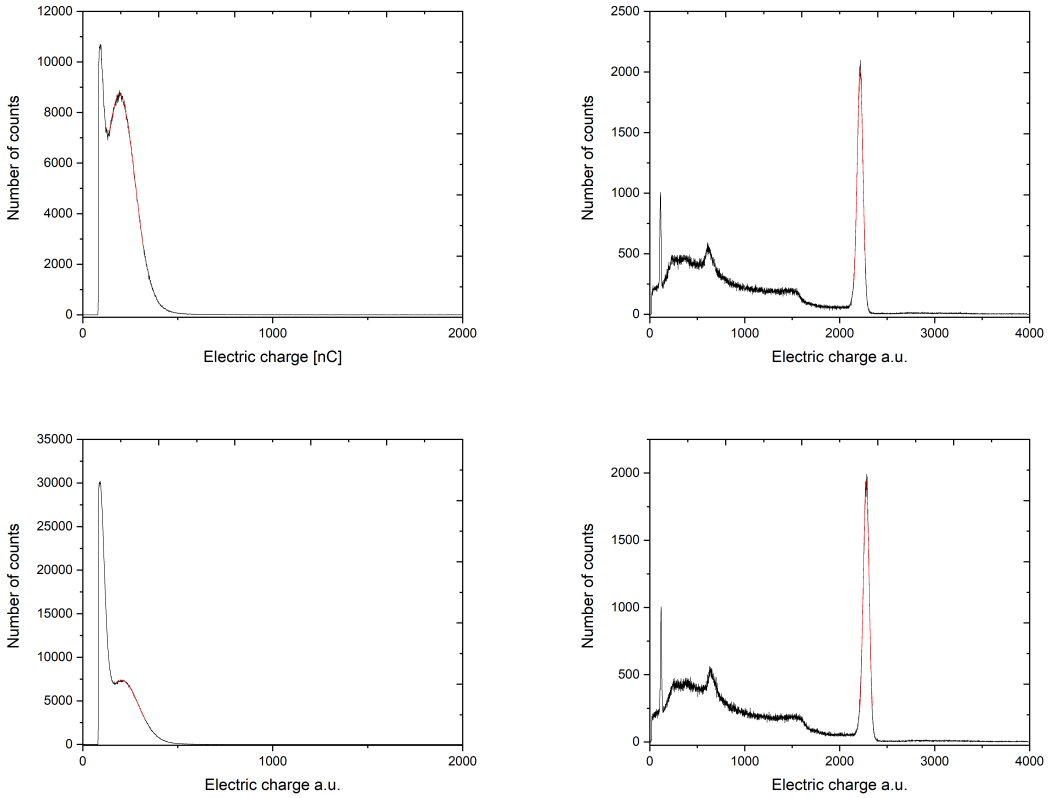

Figure 26: The charge distribution for photoelectrons measurements (left panels) and for gamma quanta from ^{137}Cs source. The upper part of the figure corresponds to the amplifier shaping time equal to 0,25 μs, and the lower panel shows plots for this parameter equal to 0,375 μs.

Then, using the obtained charge values, the amplification used in both types of measurements and quantum efficiency fo the used PMT, the light output was calculated. Dividing the charge value for Cesium by the value for the photoelectron and taking the correction for the amplifier gain, the number of photoelectrons corresponding to the peak of full absorption was obtained. This number was divided by

the photopic energy (in MeV) and the quantum efficiency of the photomultiplier was also taken into account (the probability that when a photon hits the photocathode, it will knock out an electron).

The average charge measured for one photoelectron can be expressed as:

$$Q_{pe} = Q_{tpe} \cdot W_1 \tag{12}$$

where Q_{tpe} - real charge, W_1 - total signal amplification.
Similarly, the mean charge registered in the ^{137}Cs peak of full absorption amounts to:

$$Q_{Cs} = N_{pe} \cdot Q_{tpe} \cdot \epsilon \cdot W_2 \tag{13}$$

where N_{pe} - average number of produced photons, ϵ - the probability that a single photon striking the photocathode will knock out an electron, W_2 - total signal amplification.
hence

$$N_{pe} = \frac{W_1 \cdot Q_{Cs}}{Q_{pe} \cdot \epsilon W_2 \cdot E} \tag{14}$$

where
Quantum Efficiency $\epsilon = 35\%$
Energy of photopeak E = 662keV = 0,662MeV
hence for first measurement (0,25 μs):

$$N_{pe} = 59520 \pm 146$$

and for the second measurement (0,375 μs):

$$N_{pe} = 57849 \pm 204$$

Taking into account the obtained values, the mean light output value was calculated and received:

$$N_{pe} = 58685 \pm 175$$

5. Summary

In the warfare, at the beginning of the 20th century, large amounts of poison chemical agents were used. After the end of the war, the fastest way to get rid of ammunition was to sink this arsenal in the Baltic Sea. These measures become especially dangerous when corrosive projectiles are lifted and unsealed, and dangerous compounds are spread in the water. At the Jagiellonian University, as part of the SABAT project, there is an ongoing research aiming at construction of a noninvasive detection device to detect these chemical agents on the bottom of the sea. it is based on neutron activation and measurement of the characteristic gamma rays. A significant element of this sensor is a scintillation detector, the main elements of which are a photomultiplier tube. Among the available scintillation materials, it has been shown that the LaBr crystal will be the best option for the detector. The aim of this study was characterization of the first prototype of this detector. Features like time and energy resolution, linearity, light attenuation and light output were investigated. The energy resolution was studied up to 2.2 MeV gamma rays energy using both, standard elemental sources and hydrogen activated by neutron capture. The results indicate, that for higher energy gamma quanta the resolution saturates at about 2%. The time resolution measured for the annihilation gamma quanta with energy equal to 511 keV depends on the applied PMT voltage and changes from about 0,5 ns for HV=1100 V to 0,44 ns for 1700 V. The measurements of light attenuation length revealed, that for higher vlotages the charge output of the detector decreases exponentially with decreasing distance of irradiation point to the photocathode. The nature of this effect remains not fully understood. Studies of the linearity of the response of the detector showed, that indeed its response is linear up to the energy 2,2 MeV.

References

[1] Glenn F. Know *Radiation Detection and Measurement*

[2] http://www.carbon14.pl/andrzej/Dozymetria/Wyklad06.pdf, October 2019

[3] Scintillation Products Technical Note, Saint-Global Crystals

[4] Jostein Saterstol *Characterization of ScintillationCrystals for Positron Emission Tomography*, Master Thesis, University of Bergen Faculty of Mathematics and Natural Sciences Department of Physics and Technology, 2010

[5] D.L. Bailey, D.W. Townsend, P.E. Valk, M.N. Maisey *Positron Emission Tomography*

[6] Mikhail S.Alekhin a, SandraWeber b, KarlW.Kramer b, PieterDorenbos, Journal of Luminescence 145(2014)518-524

[7] Nares Chankow *Neutron Radiography*, Department of Nuclear Engineering, Faculty of Engineering Chulalongkorn University Thailand

[8] https://www.nuclear-power.net/nuclear-power

[9] https://www.britannica.com/science/neutron

[10] T. Kasperek, *Czas Morza* 1, 15 (2001)

[11] M. Silarski, P. Moskal, FOTON 112, 15 (2011)

[12] L. Kazmierczak, et al., Acta Phys. Polon. A 127, 1540 (2015)

[13] M. Silarski, P. Moskal, Patent nr PL225474

[14] K. Fiałkowski, FOTON **120**, 4 (2013)

[15] http://www.if.pw.edu.pl/ pluta/pl/dyd/mfj/zal03/bilski/index.html, December 2019

[16] Z. Wróbel, A. Budziak, H. Hrynkiewicz, L. Jarczyk *Ćwiczenia laboratoryjne z fizyki jądrowej w pracowni studenckiej Instytutu Fizyki Uniwersytetu Jagiellońskiego*, Wydawnictwo Uniwersytetu Jagiellońskiego, Kraków, 1979

[17] M. Gierlik, S.Borsuk, Z.Guzik, Nuclear Instruments and Methods in Physics Research A834(2016)16–23

[18] www.its.bldrdoc.gov, July 2020

[19] J. Glodo, W. W. Moses, W. M. Higgins, E. V. D. van Loef, P. Wong, S. E. Derenzo, M. J. Weber, and K. S. Shah, IEEE TRANSACTIONS ON NUCLEAR SCIENCE, VOL. 52, NO. 5, OCTOBER 2005

[20] Valkovic, D. Sudac, D. Matika and R. Kollar,An Underwater System for Threat Material Detection,IFAC Proc. Vol.40(2007) 13.